Journal of Hazardous Materials 172 (2009) 792–801

Contents lists available at ScienceDirect

Journal of Hazardous Materials

journal homepage: www.elsevier.com/locate/jhazmat

Adsorption behaviors of Hg(II) on chitosan functionalized by amino-terminated hyperbranched polyamidoamine polymers

Fang Ma, Rongjun Qu*, Changmei Sun, Chunhua Wang, Chunnuan Ji, Ying Zhang, Ping Yin

School of Chemistry & Materials Science, Ludong University, Shandong 264025, China

ARTICLE INFO

Article history:
Received 21 April 2009
Received in revised form 16 July 2009
Accepted 17 July 2009
Available online 24 July 2009

Keywords:
Functionalized chitosan
Amino-terminated hyperbranched polyamidoamine polymers
Adsorption
Hg(II)
Isothermal
Kinetic

ABSTRACT

The adsorption behaviors of Hg(II) on adsorbents, chitosan functionalized by generation 1.0–3.0 of amino-terminated hyperbranched polyamidoamine polymers (denoted as CTS-1.0, CTS-2.0 and CTS-3.0, respectively), were studied. The optimum pH corresponding to the maximum adsorption capacities was found to be 5.0 for the three adsorbents. The experimental equilibrium data of Hg(II) on the three adsorbents were fitted to the Freundlich and the Langmuir models, and it is found that the Langmuir isotherm was the best fitting model to describe the equilibrium adsorption. The kinetics data indicated that the adsorption process of Hg(II) ions on CTS-1.0, CTS-2.0 and CTS-3.0 were governed by the film diffusion and followed pseudo-second-order rate model. Thermodynamic analysis and FTIR analysis revealed that the adsorption behaviors of Hg(II) ions on the three adsorbents could be considered as spontaneous, endothermic and chemical sorption process, resulting in their higher adsorption capacities at higher temperature.

1. Introduction

Mercury, known as a kind of remarkably toxic and non-biodegradable metal, can be generated by several sources, resulting in contamination of atmospheric and aquatic systems [1]. It is mobilized through a combination of natural processes such as volcanic action and erosion of mercury-containing sediments as well as through a range of anthropogenic activities such as metal plating facilities, mining operations and tanneries [2]. Exposure to mercury leads to different toxic effects in the body, including neurological and renal disturbances, inhibition of enzyme activity and cell damage [3,4]. Consequently, removal of mercury from effluents is very important.

The conventional treatments for mercury-contained effluents consist of chemical precipitation, coagulation, lime softening, reverse osmosis, ion-exchange. However, these methods sometimes suffer from problems such as high costs and production of highly toxic sludge. As an alternative to these treatment methods, adsorption is considered to be an effective and economical method for removal of Hg(II) from waste water [5–8]. The adsorption capacity of several low-cost adsorbents, such as biopolymers which can be obtained from renewable sources, has been investigated [2,9].

Among these biopolymers, chitosan has proved to be an extremely promising material. Chitosan (CTS), an alkaline deacetylated product of chitin, was used extensively due to its high hydrophilicity, nontoxicity, abundance in nature, biocompatibility, and biodegradability. A large number of hydroxyl and amino groups with high activity presented on chitosan can act as adsorption sites. However, its characteristics, including low porosity, soft in its natural form and having a tendency to agglomerate and form gels, pose a problem in wastewater treatment processes when chitosan was used for the removal of metal ions. Recently, great attention have been paid to the chemical modification of the surface of chitosan with certain functional groups, as it can evidently improve the physical and chemical properties of chitosan [10–12].

In recent years, hyperbranched polymers represented by 'dendrimers' have received considerable attention because of their multifunctional properties and high potentials in medical applications, host–guest chemistry, and dendritic catalysts [13]. Introduction of hyperbranched polymers into CTS will result in many kinds of novel functional materials [14–16].

In our previous work [17], a series of ester- and amino-terminated chitosan functionalized with dendrimer-like PAMAM polymers were synthesized via a divergent method. Their adsorption capacities for Au^{3+}, Pd^{2+}, Pt^{4+}, Ag^{+}, Cu^{2+}, Zn^{2+}, Hg^{2+}, Ni^{2+} and

* Corresponding author. Tel.: +86 535 6673982.
E-mail addresses: rongjunqu@sohu.com, qurongjun@eyou.com (R. Qu).

0304-3894/$ – see front matter © 2009 Elsevier B.V. All rights reserved.
doi:10.1016/j.jhazmat.2009.07.066

Cd^{2+} were investigated. As a further investigation, the present paper aimed to give detailed results of the adsorption properties for Hg(II) on amino-terminated chitosan functionalized with dendrimer-like polyamidoamine polymers. The effect of acidity on adsorption, the corresponding adsorption kinetics and thermodynamics were investigated.

2. Materials and methods

2.1. Materials and methods

Chitosan functionalized with amino-terminated dendrimer-like polyamidoamine (PAMAM) polymers (CTS-1.0, CTS-2.0 and CTS-

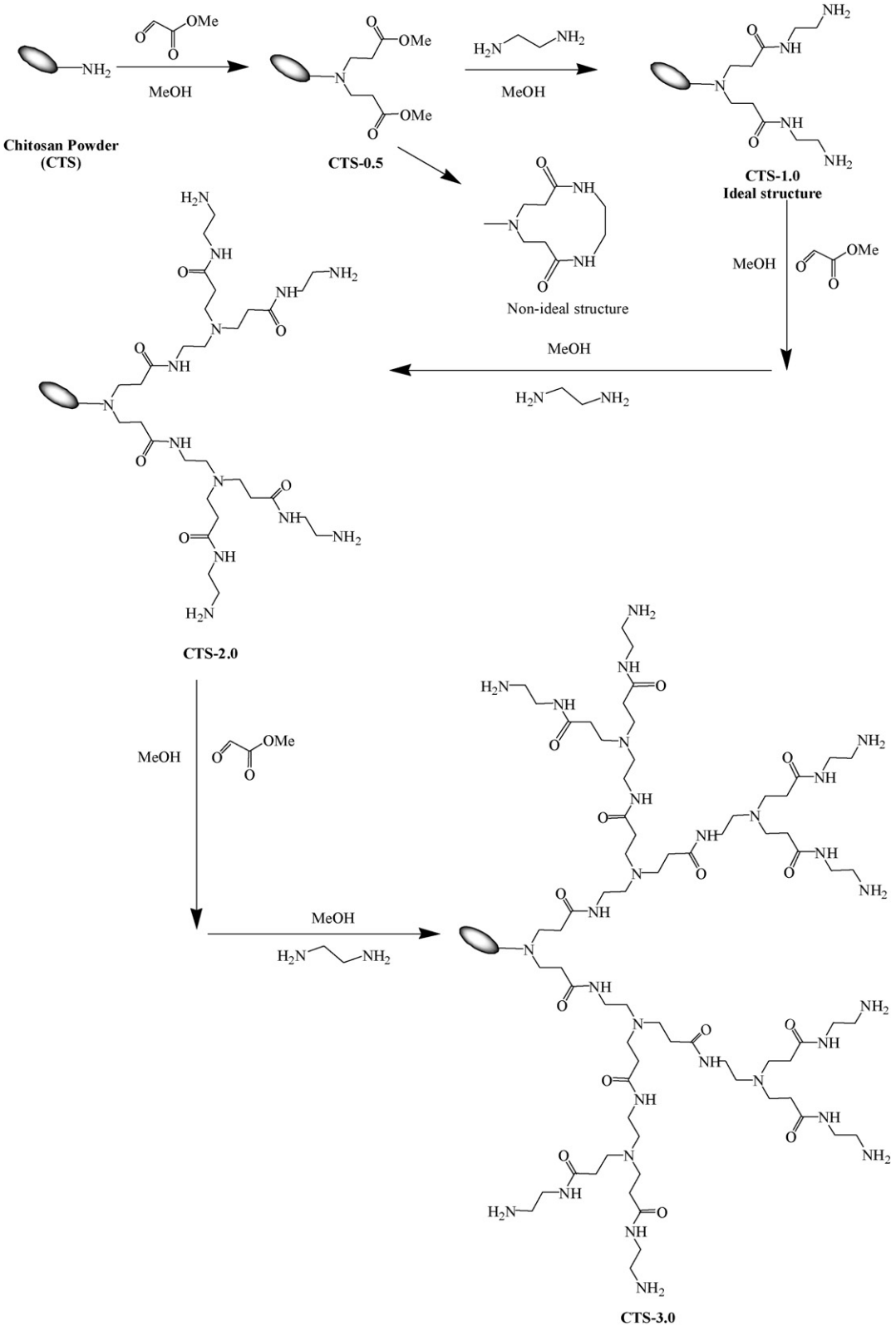

Fig. 1. The synthesis of CTS-1.0, CTS-2.0 and CTS-3.0.

3.0) was prepared according to our previous work [17], as shown in Fig. 1. Stock solutions of Hg(II) (0.1 mol L^{-1}) were prepared by dissolving $Hg(NO_3)_2{\cdot}H_2O$ in 3% HNO_3 to avoid hydrolysis. Nitric acid solution and acetic acid/sodium acetate buffer solution were used for pH adjustment. All the reagents were analytical grade and distilled water was used to prepare all the solutions.

Infrared spectra (FTIR) of samples were obtained in the range of 4000–400 cm^{-1} with a resolution of 4 cm^{-1}, by accumulating 32 scans using a Nicolet MAGNA-IR 550 (series II) spectrophotometer. KBr pellets were used for solid samples. The concentration of Hg(II) was determined using a 932B-model atomic absorption spectrometer (AAS, GBC, Australia), equipped with air–acetylene flame. The operating parameters are as follows: lamp current, 3.0 mA; slit width, 0.5 nm; wavelength, 253.7 nm; sensitivity, 1.60 μg mL^{-1}.

2.2. Adsorption experiments

Batch adsorption experiments were carried out by shaking 0.05 g of adsorbent with 20 mL of an aqueous solution of metal ions at a fixed concentration (250.74, 501.48, 1002.59, 1504.425 or 2005.90 mg L^{-1}), desired pH and temperature in a THZ-C-1 shaking incubator. The agitation rate was 100 rpm. After adsorption, the adsorbent was filtrated and the concentration of Hg(II) ions in filtrate was determined using atomic absorption spectrophotometer (GBC-932). Before all adsorption experiments, swelling experiments were conducted in order to increase the adsorption capacities. In these experiments, 0.05 g of adsorbents was swollen for 3 h in 19 mL of buffer solution at desired pH.

2.3. Effect of pH on adsorption

The adsorption experiments were performed at pH 1.0–6.0 and 25 °C by shaking 0.05 g of adsorbents with 20 ml (1002.95 mg L^{-1}) Hg(II) ion solution for 24 h at 100 rpm. The solutions used for adjusting the pH values of the medium were nitric acid solution (pH 1.0–2.0) and acetic acid/sodium acetate buffer solutions (pH 3.0–6.0). For comparison, two sets of adsorption experiments were carried out with swollen adsorbent and non-swollen adsorbent. The amount of the metal adsorbed (mg) per unit mass of CTS-1.0, CTS-2.0, CTS-3.0 (g), q_e, was obtained using the equation

$$q_e = \frac{(C_0 - C_e)V}{W} \quad (1)$$

where C_0 and C_e are the initial and equilibrium concentrations of the metal ions (mg mL^{-1}), respectively, V is the volume of the solution (mL); and W is the weight of adsorbents (g) (CTS-1.0, CTS-2.0, CTS-3.0).

2.4. Adsorption isotherms

The adsorption isotherms were investigated using 0.05 g of adsorbents with various Hg(II) ion concentrations (250.74–2005.9 mg L^{-1}) and a contact time of 24 h at pH 5.0, 25 °C.

2.5. Adsorption kinetics

The adsorption kinetics was studied using 0.05 g of adsorbents at pH 5.0, 5–35 °C. The initial Hg(II) ions concentration was 1002.95 mg L^{-1}. At various time intervals, the adsorbent was filtrated and the concentrations of Hg(II) ions in solutions were determined.

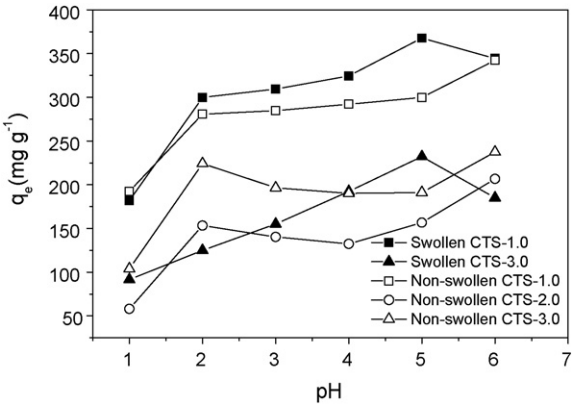

Fig. 2. Effect of pH on the adsorption of Hg(II) on swollen adsorbents (CTS-1.0, CTS-3.0) and non-swollen adsorbents (CTS-1.0, CTS-2.0 and CTS-3.0). Test conditions: 25 °C, initial Hg(II) ion concentration of 1002.95 mg L^{-1}.

3. Results and discussion

3.1. Effect of pH on adsorption

As we know, the pH of a solution is commonly an important parameter affecting adsorption of metal ions on adsorbents, as it not only affects metal species in solution but also influences the surface properties of the adsorbents in terms of dissociation of functional groups and surface charges. Therefore, the effect of solution pH on the adsorption capacities of Hg(II) on the three adsorbents (CTS-1.0, CTS-2.0 and CTS-3.0) was investigated. At the same time, the effect of swelling the adsorbents in solution was investigated choosing CTS-1.0 and CTS-3.0 as representatives. As shown in Fig. 2, the three non-swollen adsorbents exhibited good adsorption capacities for Hg(II) at the pH range of 2.0–6.0, while the adsorption capacities of swollen adsorbents were much higher than those of non-swollen adsorbents. The reason is that Hg(II) adsorbed on the surface of non-swollen adsorbents hindered the diffusion of other Hg(II) ions. For swollen adsorbents, mercury (II) could easily access to the internal active sites, due to the expansion of pores in adsorbents after the swelling step. Obviously, swelling experiments were very necessary for improving the adsorption capacities.

Moreover, the adsorption capacities at adsorption equilibrium increased with the increase of the solution pH values, particularly in the pH range of 1.0–5.0. It was thought that the lower adsorption capacities of Hg(II) ions at low solution pH values was due to the competitive coordination effect of the H^+ ions with $-NH_2$ on the surface of adsorbents [18].

The maximum adsorption capacities were achieved at pH 5.0 in the range of 1.0–6.0 examined. Consequently, all the following experiments were performed at pH 5.0 using swollen adsorbent.

3.2. Adsorption isotherms

The adsorption behaviors of Hg(II) ion on CTS-1.0, CTS-2.0, and CTS-3.0 at pH 5.0 and 25 °C were shown in Fig. 3. In order to well understand the adsorption behaviors, herein we employed Langmuir and Freundlich equations to fit the experimental data. The Langmuir equation can be expressed as:

$$\frac{C_e}{q_e} = \frac{C_e}{q} + \frac{1}{qK_L} \quad (2)$$

where q_e is the equilibrium concentration of Hg(II) ion on the adsorbent (mg g^{-1}), C_e is the equilibrium concentration of Hg(II) ion in solution (mg L^{-1}), q is the maximum capacity of adsorbent (mg g^{-1}), and K_L is the Langmuir adsorption constant (L mg^{-1}). The Freundlich equation, which is an empirical equation used to

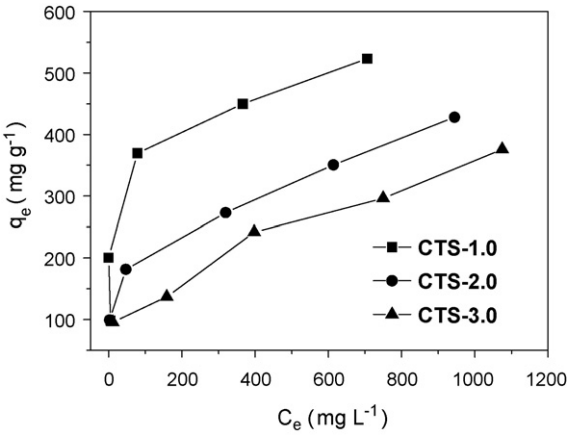

Fig. 3. Adsorption isotherms of Hg(II) on CTS-1.0, CTS-2.0, and CTS-3.0 at 25 °C.

Table 1
Parameters of Langmuir and Freundlich isotherm for adsorption of Hg(II) on the adsorbents (CTS-1.0, CTS-2.0, CTS-3.0) at 25 °C.

Adsorbents	Freundlich			Langmuir		
	n	K_F (L mg^{-1})	R^2	q_m (mg g^{-1})	K_L (L mg^{-1})	R^2
CTS-1.0	2.9886	65.31	0.6985	526.32	0.04257	0.9933
CTS-2.0	4.2340	76.81	0.9830	431.03	0.01221	0.9610
CTS-3.0	3.4014	41.50	0.9014	413.22	0.004817	0.9211

describe heterogeneous adsorption systems, can be represented as follows:

$$\ln\ q_e = \ln K_F + \frac{\ln C_e}{n} \quad (3)$$

where q_e is the equilibrium concentration of Hg(II) ions on the adsorbent (mg g^{-1}), C_e is the equilibrium concentration of Hg(II) ion in solution (mg L^{-1}), K_F is Freundlich constant (L mg^{-1}), and n is the heterogeneity factor.

According to Eqs. (2) and (3), the corresponding Langmuir and Freundlich constants and correlation coefficients (R^2) were listed in Table 1. It can be concluded that the equilibrium data fitted both Langmuir and Freundlich equations. From the correlation coefficients, it was found that the experiment data fitted Langmuir equation better than Freundlich equation, revealing the adsorption of Hg(II) ions on the adsorbent obeyed the Langmuir adsorption isotherm (Fig. 4). This suggests that the reaction between the adsorbent and the sorbate remained the same over the range of concentrations tested [19]. The above fact shows that the adsorption of Hg(II) on the three adsorbents is attributed to monolayer adsorption.

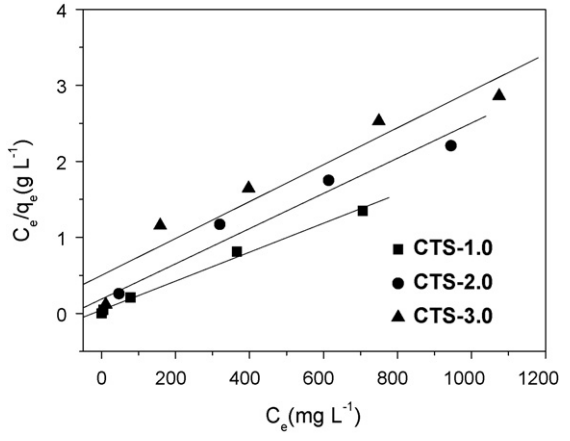

Fig. 4. Langmuir isotherms of Hg(II) on CTS-1.0, CTS-2.0, and CTS-3.0 at 25 °C.

In addition, it was noteworthy that the equilibrium concentration of Hg(II) ion on CTS-1.0 or CTS-2.0 was almost undetectable when the initial concentration of Hg(II) ion was less than 500 mg L^{-1}, revealing that the adsorbents CTS-1.0 and CTS-2.0 were quite efficient for the adsorption of Hg(II) ions.

3.3. Adsorption kinetics

Adsorption kinetics studies were carried out to determine the uptake rates of Hg(II) on the adsorbents and get access to the equilibrium time. Fig. 5 shows the adsorption kinetics of CTS-1.0, CTS-2.0 and CTS-3.0 for Hg(II) at 5–35 °C.

As shown in Fig. 5, the adsorption capacities of CTS-1.0, CTS-2.0 and CTS-3.0 for Hg(II) at 5–35 °C increased with the extension of contact time. From these data, the equilibrium time for the adsorp-

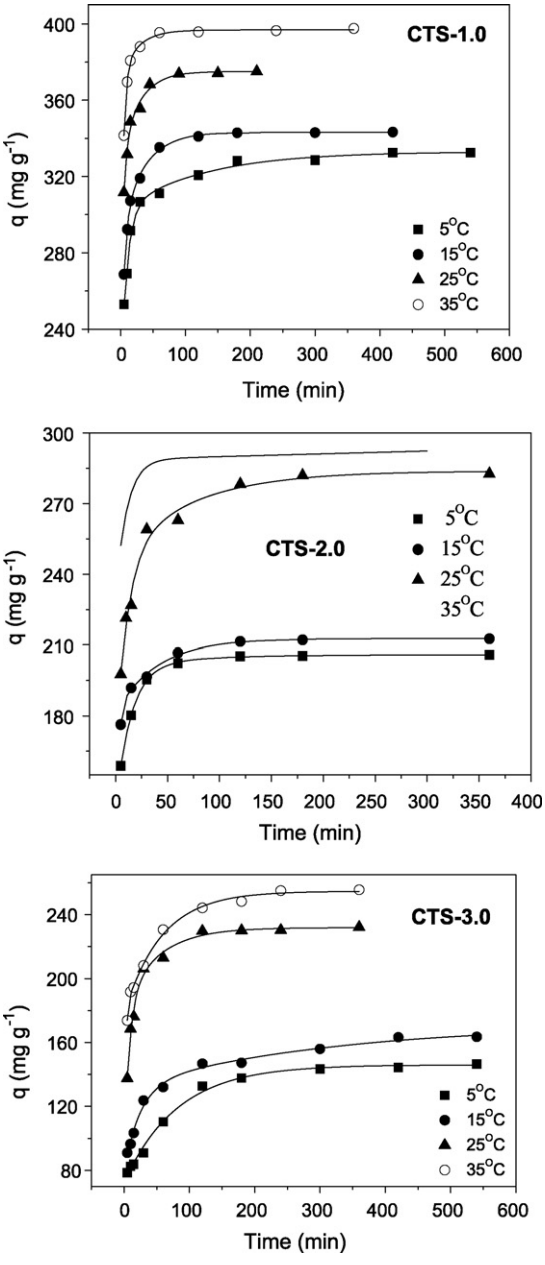

Fig. 5. Adsorption kinetics of Hg(II) on CTS-1.0, CTS-2.0, and CTS-3.0 at different temperatures.

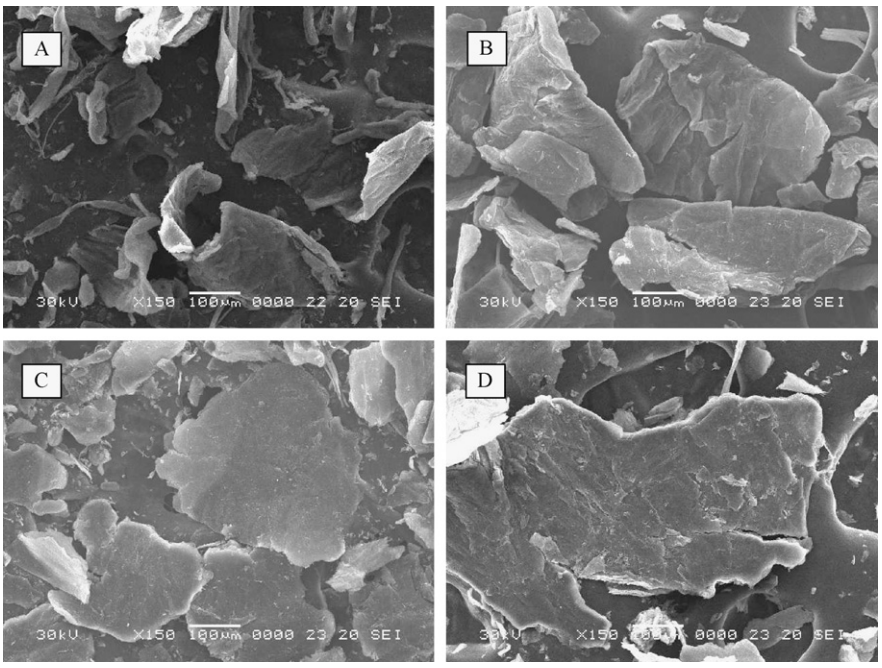

Fig. 6. SEM images showing the overall morphologies of (A) CTS, (B) CTS-1.0, (C) CTS-2.0 and (D) CTS-3.0.

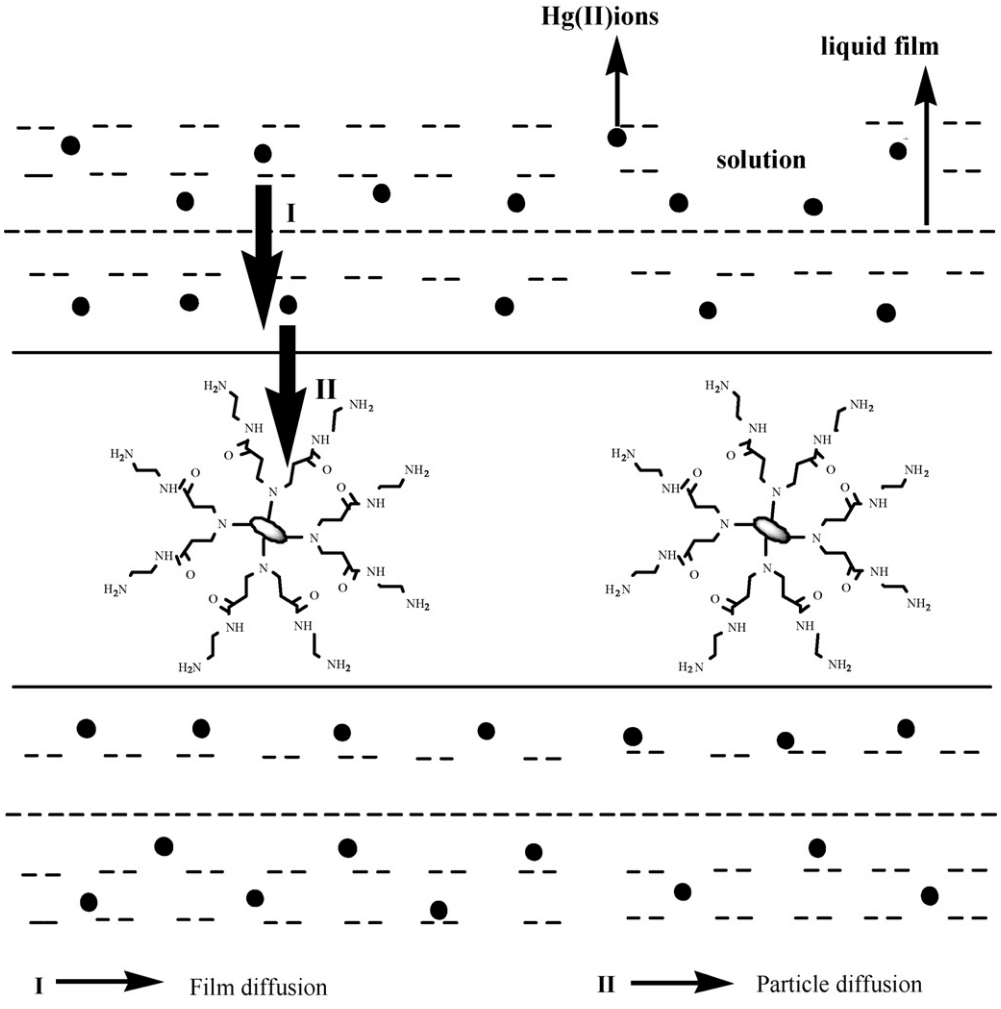

Fig. 7. The diffusion steps of Hg(II) ion.

Table 2
Linearized forms of the homogeneous diffusion model (HDM) and shrinking core model (SCM) for ion-exchange/sorption kinetics (X represents the fractional approach to equilibrium: $q(t)/q_e$).

Model and controlling step	$F(X)$, y-axis	x-axis
HDM-FD	$-\ln(1-X)$	t
HDM-PD	$-\ln(1-X^2)$	t
SCM-FD	X	$\int_0^t C(t)\ dt$
SCM-PD	$3-3(1-X)^{2/3}-2X$	$\int_0^t C(t)\ dt$
SCM-CR	$1-(1-X)^{1/3}$	$\int_0^t C(t)\ dt$

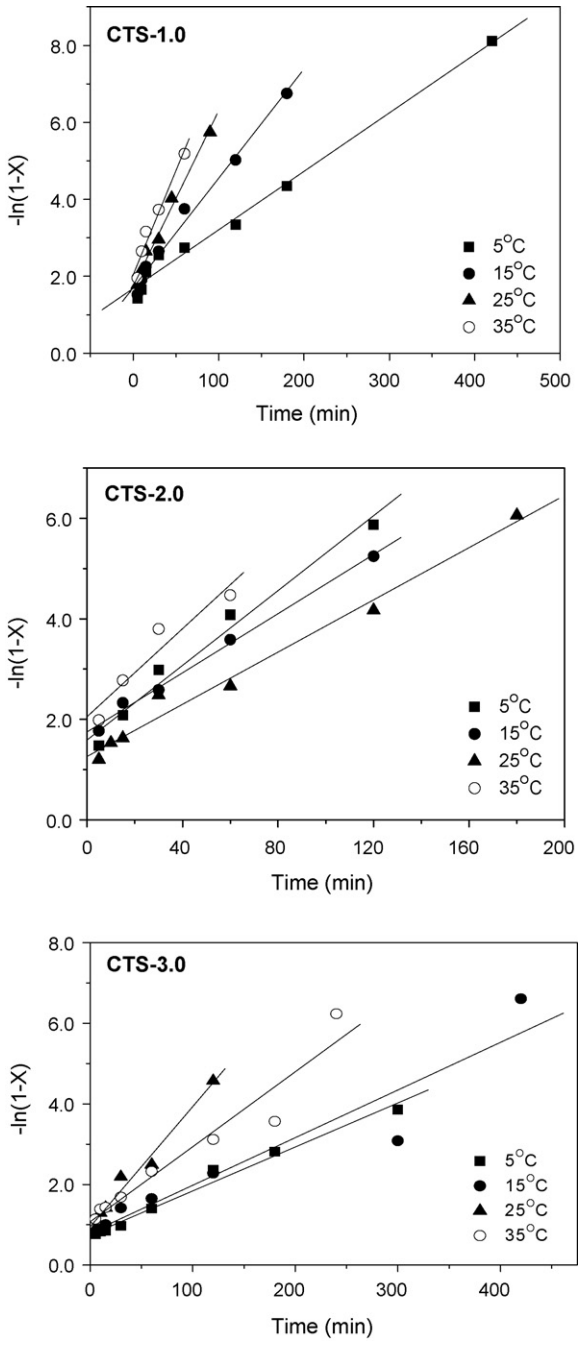

Fig. 8. Linearization of kinetic data using homogeneous diffusion model (HDM) with film diffusion (FD) of Hg(II) adsorption on CTS-1.0, CTS-2.0, and CTS-3.0.

tion of Hg(II) under the given test conditions can be evaluated to be 2 h for CTS-1.0 and 3 h for CTS-2.0 and CTS-3.0. For all the three adsorbents, the adsorption capacities increased with the increase of temperature. The order of adsorption capacities at a given temperature was: CTS-1.0 > CTS-2.0 > CTS-3.0, indicating the adsorption capacities decreased with the increase of the generation number of hyperbranched polyamidoamine polymers.

In general, the adsorption procedure of adsorbents for metal ions is considered to take place through two mechanisms of film diffusion and particle diffusion [20,21]. Usually, the Boyd et al. [20] and Reichenberg [21] equations are used to analyze the experimental data for distinguishing film diffusion from particle diffusion controlled adsorption, but the model is suitable to spherical sorbents. It was found that in this work the higher the generation number, the finer the product particles. The fine particles were then treated as spherical materials, and the Boyd and Reichenberg equations were ever attempted to analyze the experimental data in this work, but the results were not ideal (the results were not shown). Morphologies of the CTS and the products obtained from each synthesis step were characterized by SEM. As shown in Fig. 6, compared to the relatively thin and curled flake before functionalization, the products (CTS-1.0, CTS-2.0 and CTS-3.0) became thick and stretched, but the overall morphology of products was still flake-like. The model which is suitable for flake-like materials is expected.

The uptake of adsorbate by the sorbent from solutions involves several steps, including (i) bulk diffusion, (ii) film diffusion, (iii) intraparticle diffusion, and (iv) sorption and/or ion-exchange process. The complete modeling of adsorption is very complex because it is necessary to take into account various components, including not only diffusion steps but also boundary conditions (e.g. the equilibrium at the solid–liquid surface). It was proposed that the conventional models were less accurate for chitosan flake material, whose shape (tablets rather than spheres) and porosity (weak porosity) are very different from conventional materials [22]. To solve the problem, simplified models have been developed. Guibal [22] reviewed various simple kinetic models, including the homogeneous diffusion model (HDM) based on Fick's law controlled by film diffusion (FD) or particle diffusion (PD) and the shrinking core model (SCM) controlled by film diffusion, particle diffusion, or chemical reaction (CR). As shown in Fig. 7, in HDM, the species in the solution diffuse across the liquid film surrounding the particle (this step was defined as (I) in Fig. 7), transfer across the solution/particle surface, diffuse into the bulk of the particle, and possibly interact with the ligands fixed on the particle surface (the step (II)). In SCM, if the rate of ion exchange is governed by the diffusion through the shell region at quasi-steady-state conditions, e.g., this model assumes a sharp boundary between the reacted shell of the particle and the unreacted core (Table 2) [23]. In this paper, the homogeneous diffusion model controlled by film diffusion (HDM-FD) was

Table 3
Parameters of homogeneous diffusion model (HDM) with film diffusion (FD).

Adsorbents	T (°C)	Linear equation	Correlation coefficient, R^2	Intercept error
CTS-1.0	5	$y = 0.0152x + 1.6885$	0.9876	0.1174
	15	$y = 0.0284x + 1.7054$	0.9878	0.1215
	25	$y = 0.0455x + 1.7411$	0.9831	0.1300
	35	$y = 0.0540x + 2.0422$	0.9599	0.1983
CTS-2.0	5	$y = 0.0372x + 1.5872$	0.9776	0.2010
	15	$y = 0.0294x + 1.7490$	0.9942	0.0803
	25	$y = 0.0260x + 1.2600$	0.9828	0.1322
	35	$y = 0.0438x + 2.0516$	0.9128	0.3300
CTS-3.0	5	$y = 0.0109x + 0.7472$	0.9841	0.0755
	15	$y = 0.0118x + 0.7982$	0.9082	0.2900
	25	$y = 0.0298x + 0.9505$	0.9746	0.1365
	35	$y = 0.0186x + 1.0742$	0.9360	0.2323

attempted to describe the adsorption kinetics of Hg(II) on CTS-1.0, CTS-2.0, and CTS-3.0, and the results are shown in Fig. 8. The parameters of HDM-FD model were given in Table 3. As can be seen from Table 3, the HDM-FD model provided good correlation coefficients R^2 for all adsorbents almost at the temperature range studied, suggesting the HDM-FD model was suitable to describe the adsorption kinetics of CTS-1.0, CTS-2.0 and CTS-3.0 for Hg(II).

3.4. Adsorption kinetics models

The kinetics parameters, such as the rate constants and equilibrium adsorption capacities, which can provide valuable insights into the design of water treatment process, are of great importance for the application of adsorbents. Both pseudo-first-order and pseudo-second-order models can be used to express the adsorption process of CTS-1.0, CTS-2.0 and CTS-3.0 for Hg(II).

The pseudo-first-order and pseudo-second-order models can be expressed by Eqs. (4) and (5), respectively:

$$\log(q_e - q) = \log\ q_e - \frac{k_1}{2.303}t \tag{4}$$

$$\frac{t}{q} = \frac{1}{k_2 q_e^2} + \frac{1}{q_e}t \tag{5}$$

where q_e (mg g^{-1}) is the amount of metal adsorbed at equilibrium per unit weight of adsorbent, q (mg g^{-1}) is the amount of metal adsorbed at any time, k_1 (min^{-1}) and k_2 (g mmol^{-1} min^{-1}) are the rate constants of pseudo- first-order and pseudo-second-order adsorption.

The plots of $\log(q_e - q)$ versus t and t/q versus t were employed to test the pseudo-first-order and pseudo-second-order models, the results of testing the pseudo-second-order models were shown in Fig. 9. The fitting results were given in Table 4.

As can be seen from Table 4, the pseudo-second-order model provided better correlation coefficients than the pseudo-first-order model for all the adsorbents at any temperature studied, suggesting the pseudo-second-order model was more suitable to describe the adsorption kinetics of CTS-1.0, CTS-2.0 and CTS-3.0 for Hg(II). At the same time, the fact of equilibrium adsorption capacities calculated ($q_{e,\mathrm{cal}}$) depending on the pseudo-second-order model much closer to the experimental data $q_{e,\mathrm{exp}}$ also proved the suitability of pseudo-second-order model.

3.5. Determination of ΔG, ΔH and ΔS

Data from the kinetics adsorption experiments were used to determine the values of ΔH and ΔS. The partition coefficients (K_c) of each temperature were derived from the following equation:

$$K_c = \frac{C_{Ae}}{C_e} \tag{6}$$

where C_e is the equilibrium concentration in solution (mg L^{-1}) and C_{Ae} the solid phase concentration at equilibrium (mg L^{-1}).

By plotting $\ln K_c$ versus $1/T$ as shown in Fig. 10, the changes of enthalpy and entropy could be obtained from the slope and y-intercept using the following Eq. (7):

$$\ln K_c = -\left(\frac{\Delta H}{R}\right)\left(\frac{1}{T}\right) + \frac{\Delta S}{R} \tag{7}$$

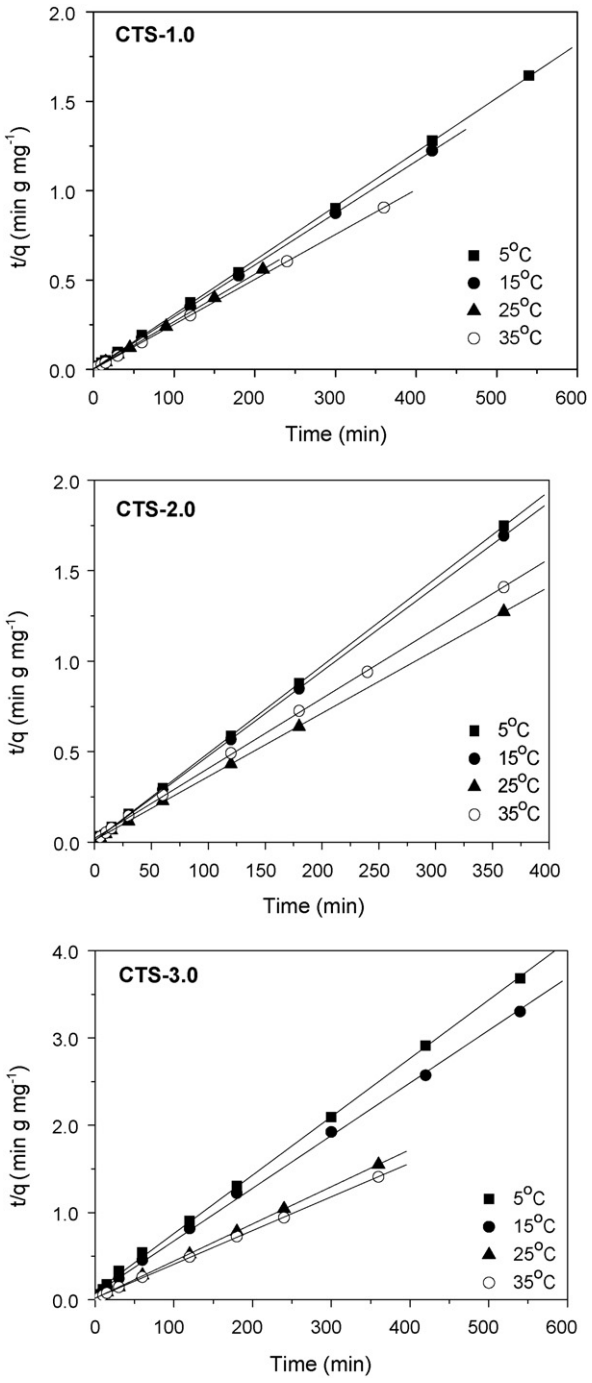

Fig. 9. Pseudo-second-order kinetic plots of Hg(II) on CTS-1.0, CTS-2.0, and CTS-3.0 at different temperature.

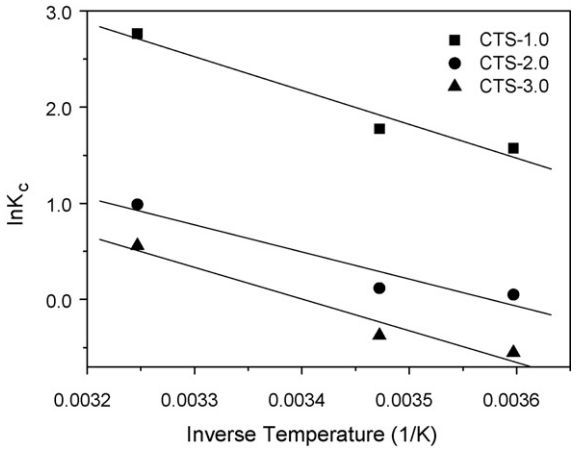

Fig. 10. Enthalpy and entropy change determination for Hg (II) adsorption to CTS-1.0, CTS-2.0 and CTS-3.0.

Table 4
The adsorption kinetic rate constants for CTS-1.0, CTS-2.0, and CTS-3.0 at different temperature.

Adsorbents	T (°C)	$q_{e,exp}$ (mg g^{-1})	Pseudo-first-order model			Pseudo-second-order model		
			$q_{e,cal}$ (mg g^{-1})	k_1 (min^{-1})	R^2	$q_{e,cal}$ (mg g^{-1})	k_2 (g mg^{-1} min^{-1})	R^2
CTS-1.0	5	332.52	59.76	0.013357	0.9178	331.12	0.001550	1
	15	343.30	42.42	0.019806	0.8997	334.83	0.001690	1
	25	375.02	44.93	0.030630	0.8971	377.36	0.002080	1
	35	397.60	20.15	0.014739	0.6997	398.41	0.003405	1
CTS-2.0	5	205.84	31.03	0.028097	0.9292	207.04	0.003060	1
	15	212.54	32.26	0.025333	0.9823	213.68	0.002740	1
	25	282.62	80.17	0.026024	0.9828	285.71	0.001080	0.9999
	35	292.58	17.78	0.014509	0.6991	259.07	0.000720	1
CTS-3.0	5	146.54	61.77	0.008982	0.9555	149.48	0.000502	0.9993
	15	163.48	76.91	0.011745	0.8957	165.56	0.000522	0.9990
	25	232.20	59.88	0.017503	0.8781	234.74	0.000992	0.9999
	35	255.54	87.3	0.018654	0.9360	259.07	0.000719	0.9997

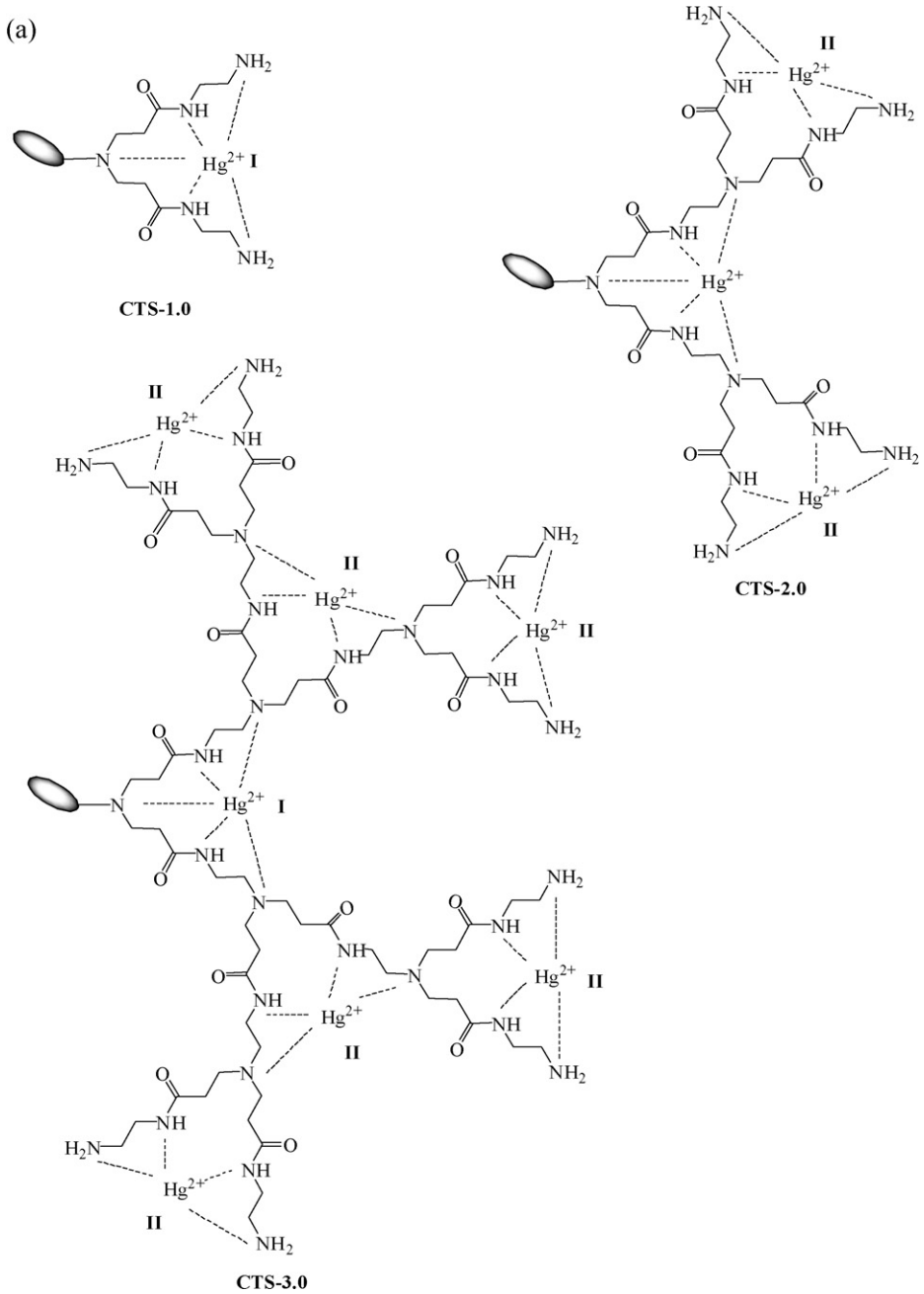

Fig. 11. Proposed structure of Hg^{2+} chelation on CTS-1.0, CTS-2.0 and CTS-3.0.

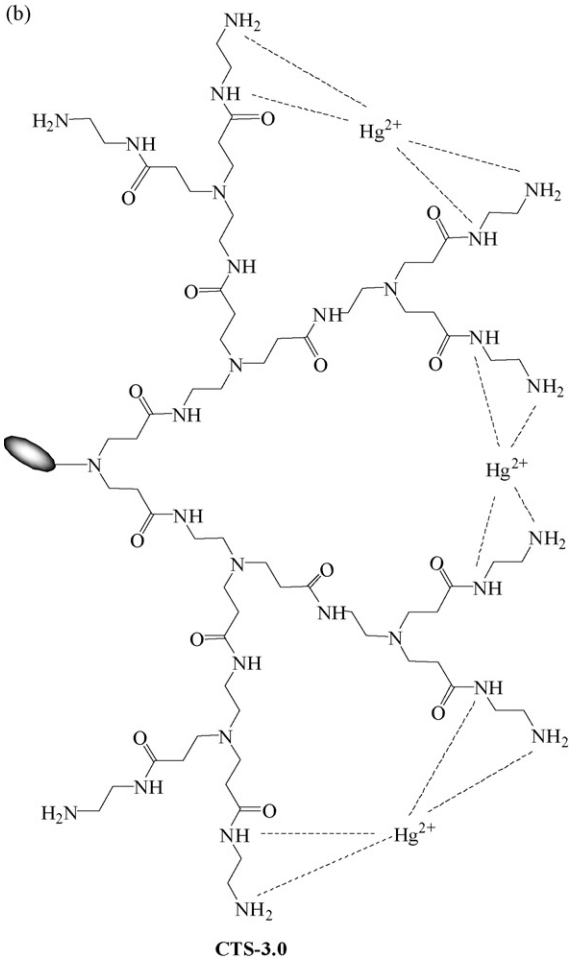

Fig. 11. (*Continued*).

where R is the gas constant (8.314 J mol^{-1} K^{-1}), and T is the temperature in Kelvin. ΔG was calculated at each temperature by Eq. (8):

$$\Delta G = \Delta H - T\Delta S \quad (8)$$

The Gibbs free energy change (ΔG), enthalpy change (ΔH) and entropy change (ΔS) were shown in Table 5. The enthalpy change for Hg(II) adsorption on CTS-1.0, CTS-2.0, and CTS-3.0 were 29.250, 23.427 and 27.399 kJ mol^{-1}, respectively, indicating that in all cases Hg(II) ions adsorption on CTS-1.0, CTS-2.0, and CTS-3.0 were endothermic. This result was consistent with the case that, for each adsorbent, the adsorption capacities of Hg(II) ions increased with the increasing of temperature. Moreover, enthalpy change value is useful for distinguishing physisorption or chemisorption. Physisorption is typically associated with heats of adsorption in the 2.1–20.9 kJ mol^{-1} range, while chemisorption is typically associated with much larger ΔH values (i.e. 20.9–418.4 kJ mol^{-1}) [24,25]. The sorption heat of Hg(II) are in the range of 20.9–418.4 kJ mol^{-1}, which suggests that the adsorption processes of Hg(II) on CTS-1.0, CTS-2.0, and CTS-3.0 were taken place via chemisorptions.

Table 5
Isothermal parameters of Hg(II) adsorption on CTS-1.0, CTS-2.0, and CTS-3.0.

Adsorbents	T (°C)	ΔG (kJ mol^{-1})	ΔH (kJ mol^{-1})	ΔS (J mol^{-1})
CTS-1.0	5	−3.42	29.25	117.52
	15	−4.60		
	25	−5.77		
	35	−6.95		
CTS-2.0	5	0.14	23.43	83.76
	15	−0.69		
	25	−1.53		
	35	−2.37		
CTS-3.0	5	1.49	27.40	93.20
	15	0.56		
	25	−0.37		
	35	−1.30		

It is well known that N ligand possesses affinity to adsorb Hg(II) which belongs to soft acid. The adsorbents (CTS-1.0, CTS-2.0, CTS-3.0) possess tertiary amine, secondary amine and primary amine which can serve as a ligand for Hg complexation under moderate affinity. The proposed chelation structures of Hg^{2+} by adsorbents (CTS-1.0, CTS-2.0, CTS-3.0) were shown in Fig. 11(a). The Hg(II) may chelate with four N atoms (I) or five N atoms (II). Theoretically, the adsorption capacities of adsorbents for Hg(II) should increase with the increasing of generation number of dendrimer-like PAMAM polymers grafted on chitosan. However, the investigation of the fact proved the contrary (Fig. 2). This phenomenon might be explained as follows: (I) the steric hindrance and the degree of crosslinking in the structure of higher generation are higher than those of the lower generation [17], and (II) the N atoms on the surface of adsorbents chelated with Hg(II) (Fig. 11(b)), which makes it harder for Hg(II) to diffuse into the interior of higher generation polymers.

The negative ΔG values indicated the spontaneous nature of the adsorption process. The increase in ΔG values with increase in temperature shows an increased feasibility of adsorption at higher temperature. The ΔG values for the Hg(II) adsorption on CTS-1.0 were negative at 5–35 °C, indicating that the adsorption process was spontaneous. Different from CTS-1.0, the negative values of ΔG for CTS-2.0 and CTS-3.0 appeared at higher temperature ranges (i.e. 15–35 °C for CTS-2.0 and 25–35 °C for CTS-3.0), meaning that their spontaneous adsorptions only occurred at higher temperature. It is noteworthy that the values of ΔG for CTS-2.0 and CTS-3.0 at lower temperature are positive. A similar phenomenon was found in the adsorption of Au(III) on chitosan-coated magnetic nano-adsorbent by Chang and Chen [26], which was attributed by these authors to the presence of an energy barrier in the adsorption process and to the activated complex in the transition state in an excited form. The positive ΔS values suggest an increase in the randomness at the solid/solution interface during the adsorption process.

FTIR analysis is a useful technology in exploring the adsorption behaviors of metal ions on adsorbents. In order to further confirm the adsorption mechanism of CTS-1.0, CTS-2.0, and CTS-3.0 for Hg(II), the changes of characteristic absorption peaks in adsorbents before and after adsorption were investigated by FTIR. CTS-1.0 was

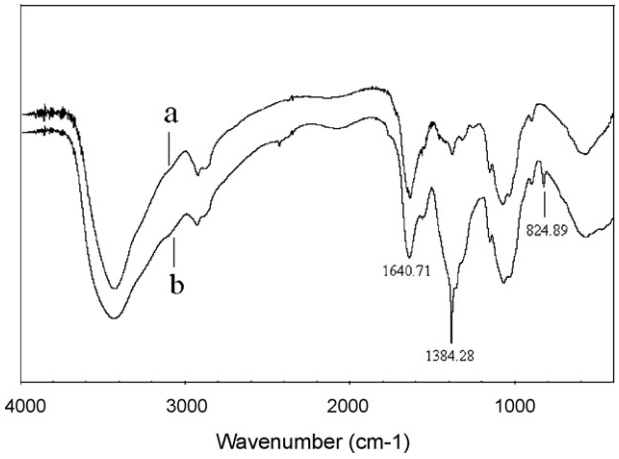

Fig. 12. FT-IR spectra of CTS-1.0 before (a) and after (b) adsorption for Hg(II).

chosen as a representative as it has similar functional groups and structures to CTS-2.0 and CTS-3.0 [17]. Fig. 12 shows a FTIR profile of CTS-1.0 before and after loading with Hg(II) ions solution. The weakening of peaks at 1640 cm^{-1} attributed to the characteristic peak of –NHCO and $–NH_2$ and appearance of new peak at 824 cm^{-1} assigned to δNH_3^+ can be considered as the evidence of the coordination of –NHCO and $–NH_2$ with Hg(II). It is also observed that a very strong new peak at 1384.28 cm^{-1} occurred in the FTIR spectrum of CTS-1.0 after adsorption in Fig. 12(b). The peak at 1384.28 cm^{-1} is a characteristic peak for the stretching vibration of NO_2 in the NO_3^- ions [27]. The results of FTIR analysis further demonstrated that the adsorption of CTS-1.0, CTS-2.0, and CTS-3.0 for Hg(II) were carried out through chemisorption mechanism, which is consistent with the deduction in Section 3.3.

4. Conclusions

The following major conclusions can be drawn based on the above study:

(1) The optimum pH corresponding to the maximum adsorption was found to be 5.0 for CTS-1.0, CTS-2.0 and CTS-3.0. The adsorption capacities of adsorbents for Hg(II) decreased with the increase of generation number of dendrimer-like PAMAM polymers grafted on chitosan.
(2) The isotherm adsorption data of the Hg(II) on adsorbents CTS-1.0, CTS-2.0 and CTS-3.0 at 25 °C were well fitted by the Langmuir model.
(3) The adsorption kinetic study indicated that pseudo-second-order rate model providing an excellent fitting of CTS-1.0, CTS-2.0 and CTS-3.0 for Hg(II) over the temperature range of 5–35 °C and the film diffusion might be involved in the adsorption process.
(4) The Hg(II) adsorptions process of CTS-1.0 was spontaneous over the temperature range studied, but those of CTS-2.0 and CTS-3.0 only at higher temperatures. All the adsorption processes exhibited endothermic, monolayer and chemical adsorption in nature.

Acknowledgements

The authors are grateful for the financial support by the Nature Science Foundation of Shandong Province (No. 2008BS04011 and No. 2005BS11010), the Nature Science Foundation of Ludong University (No. 032912, 042920, 08-CXA001, LY20072902), and Educational Project for Postgraduate of Ludong University (No. Ycx0612).

References

[1] F.M.M. Morel, A.M.L. Kraepiel, M. Amyot, The chemical cycle and bioaccumulation of mercury, Annu. Rev. Ecol. Syst. 29 (1998) 543–566.
[2] S.E. Bailey, T.J. Olin, R.M. Bricka, D.D. Adrian, A review of potentially low-cost sorbents for heavy metals, Water Res. 11 (1999) 2469–2479.
[3] J. Choong, H.P. Kwang, Adsorption and desorption characteristics of mercury (II) ions using aminated chitosan bead, Water Res. 39 (2005) 3938–3944.
[4] A. Saglam, Y. Yalchinkaya, A. Denizli, M.Y. Arica, Ö. Genc, S. Bektas, Biosorption of mercury by carboxymethyl-cellulose and immobilizes phanerochaete chrysosporium, Microchem. J. 71 (2002) 73–81.
[5] B.S. Inbaraj, J.S. Wang, J.F. Lu, F.Y. Siao, B.H. Chen, Adsorption of toxic mercury(II) by an extracellular biopolymer poly(γ-glutamic acid), Bioresour. Technol. 100 (2009) 200–207.
[6] Y.S. Ho, C.C. Wang, Sorption equilibrium of mercury onto ground-up tree fern, J. Hazard. Mater. 156 (2008) 398–404.
[7] L. Zhou, Y.P. Wang, Z.R. Liu, Q.W. Huang, Characteristics of equilibrium, kinetics studies for adsorption of Hg(II), Cu(II), and Ni(II) ions by thiourea-modified magnetic chitosan microspheres, J. Hazard. Mater. 161 (2009) 995–1002.
[8] A. Shafaei, F.Z. Ashtiani, T. Kaghazchi, Equilibrium studies of the sorption of Hg(II) ions onto chitosan, Chem. Eng. J. 133 (2007) 311–316.
[9] S. Babel, T.A. Kurniawan, Low-cost adsorbents for heavy metal uptake from contaminated water: a review, J. Hazard. Mater. 97 (2003) 219–243.
[10] T.Y. Hsien, G. Rorrer, Heterogeneous cross-linking of chitosan gel beads: kinetics, modeling and influence on cadmium ion adsorption capacity, Ind. Eng. Chem. Res. 36 (1997) 3631–3638.
[11] A.M. Donia, A.A. Atia, K.Z. Elwakeel, Selective separation of mercury(II) using magnetic chitosan resin modified with Schiff's base derived from thiourea and glutaraldehyde, J. Hazard. Mater. 151 (2008) 372–379.
[12] A.A. Atia, Studies on the interaction of mercury(II) and uranyl(II) with modified chitosan resins, Hydrometallurgy 80 (2005) 13–22.
[13] A.W. Bosman, H.M. Janssen, E.W. Meijer, About dendrimers: structure, physical properties, and applications, Chem. Rev. 99 (1999) 1665–1688.
[14] H. Sashiwa, Y. Shigemasa, R. Roy, Chemical modification of chitosan. Part 9. Reaction of *N*-carboxyethyl ester with diamines of acetal ending PMAMA dendrimers, Carbohyd. Polym. 47 (2002) 201–208.
[15] H. Sashiwa, Y. Shigemasa, R. Roy, Chemical modification of chitosan 8: preparation of chitosan-dendrimer hybrids via short spacer, Carbohyd. Polym. 47 (2002) 191–199.
[16] H. Sashiwa, Y. Shigemasa, R. Roy, Chemical modification of chitosan 11: chitosan-dendrimer hybrid as a tree like molecule, Carbohyd. Polym. 49 (2002) 195–205.
[17] R.J. Qu, C.M. Sun, C.N. Ji, C.H. Wang, H. Chen, Y.Z. Niu, C.J. Liang, Q.Y. Song, Preparation and metal-binding behaviour of chitosan functionalized by ester- and amino-terminated hyperbranched polyamidoamine polymers, Carbohyd. Res. 343 (2008) 267–273.
[18] C.K. Liu, R.B. Bai, Q.S. Ly, Selective removal of copper and lead ions by diethylenetriamine-functionalized adsorbent: behaviors and mechanisms, Water Res. 42 (2008) 1511–1522.
[19] K. Xu, W.F. Harper Jr., D.Y. Zhao, 17α-Ethinylestradiol sorption to activated sludge biomass: thermodynamic properties and reaction mechanisms, Water Res. 42 (2008) 3146–3152.
[20] G.E. Boyd, A.W. Adamson, L.S. Meyers Jr., The exchange adsorption of ions from aqueous solution by organic zeolites. II. Kinetics, J. Am. Chem. Soc. 69 (1947) 2836–2848.
[21] D. Reichenberg, Properties of ion exchange resins in relation to their structure. III. Kinetics of exchange, J. Am. Chem. Soc. 75 (1953) 589–597.
[22] E. Guibal, Interactions of metal ions with chitosan-based sorbents: a review, Sep. Purf. Technol. 38 (2003) 43–74.
[23] R.S. Juang, C.Y. Ju, Kinetics of sorption of Cu(II)-ethylenediaminetetraacetic acid chelated anions on cross-linked, polyaminated chitosan beads, Ind. Eng. Chem. Res. 37 (1998) 3463–3469.
[24] L. Deng, Y. Su, H. Su, X. Wang, X. Zhu, Sorption and desorption of lead (II) from wastewater by green algae. *Cladophora fascicularis*, J. Hazard. Mater. 143 (2007) 220–225.
[25] J.M. Smith, Chemical Engineering Kinetics, third ed., McGraw-Hill, New York, 1981, pp. 310–322.
[26] Y.C. Chang, D.H. Chen, Recovery of gold(III) ions by a chitosan-coated magnetic nano-adsorbent, Gold Bull. 39 (2006) 98–102.
[27] M. Takafuji, S. Ide, H. Ihara, Z. Xu, Preparation of poly(L-vinylimidazole)-grafted magnetic nanoparticles and their application for removal of metal ions, Chem. Mater. 16 (2004) 1977–1983.